Engineering Symposium at Bánki
(ESB 2021)
http://bgk.uni-obuda.hu/esb/2021/

Impact toughness and microstructures behavior of the Aluminum EN AW 6082 rheocasting and casting alloys in different temperatures

[1,2] Kawan M. Abdulrahman, [3] Viktor Gonda, [4] Mihály Réger

[1] *Doctoral School on Materials Sciences and Technologies Óbuda University, Budapest, Hungary,*
[2] *Sulaimani Polytechnic University, Technical College of Engineering, Department of Production Engineering & Metallurgy, Iraq,*
kawan.abdulrahman@uni-obuda.hu
[3] *Óbuda University, Bánki Faculty of Mechanical and Safety Engineering, Budapest, Hungary, gonda.viktor@bgk.uni-obuda.hu*
[4] *Óbuda University, Bánki Faculty of Mechanical and Safety Engineering, Budapest, Hungary, reger.mihaly@bgk.uni-obuda.hu*

Abstract

The rheocasting method is known as one of the techniques of Semi-solid metal (SSM). It is conducted between the states of solidus and liquidus in which a non-dendritic microstructure is created, and in a liquid matrix, it produces solid spheroids. This paper reports a Charpy Impact test which shows the Effect of Heat on the Charpy Impact toughness of the casting and the rheocasting for aluminum alloy EN AW 6082. The test samples are subjected to Charpy impact tests at different temperatures (0, 25, 40,100, -25, and -40)°C and compared the result of casting with rheocasting samples. Also, the Brinell hardness test was conducted on Aluminum EN AW 6082 and Rheocasting alloy samples at room temperature. According to ASTM standards, the scanning electron microscope (SEM) fracture obtained result; it can be noticed that the microstructure of the rheocasting sample changed more due to the work results.

The present work shows significant toughness increases for rheocasting aluminum alloy EN AW 6082 compared with casting aluminum alloy EN AW 6082 in all different temperatures. The value of rheocasting alloy toughness increased three or more times compared with casting alloy toughness. Besides, measuring the lateral dimensions of the alloy toughness after the test supported the toughness results, the variation of an explosive edge in the Charpy impact test for casting, and rheocasting samples at different temperatures compared to the edges in casting aluminum alloys. All Charpy impact tests for rheocasting samples test have higher measuring edge values than casting samples test, especially in high temperatures. The effect of the typical Brinell hardness test for rheocasting samples suggests an improvement in hardness from 95 to 125 HB.

Keywords: Semi-Solid, Rheocasting, aluminum alloy EN AW 6082, Toughness; Impact test, Charpy test, SEM test, hardness test.

1 Introduction

In an impact test, impact energy refers to the total amount of energy used. A given specimen that fractures after being tested below a high strain rate or quick loading state absorb the total energy. The Charpy test is the most popular type of impact test, and it is used in the laboratory to quantify impact energy [1-2]. The overall area under the stress-strain curve is reflected in the energy value. Furthermore, research on the link between fracture characteristics and microstructure of hypereutectic Al-Mg-Si alloy castings is included in this test. It consequently leads to a reduction in

the resistance to crack initiation, raising the accuracy of the impact values and underlining the effects of microstructure. The current work benefited from Charpy unnotched samples [3-4].

Using an internal heat absorber technique, the rheocasting process presents a method to manufacture more cost-effective components with the practice of near-net-shape for various aluminum alloys. The rheocasting process seems possible through better process control during the slurry formation [5].

The Charpy test, similarly identified as the Charpy V-notch test, is an identical high strain-rate test that determines the value of energy absorbed by an alloy through the fracture. The value of absorbed energy was measured of a given material's notch toughness and performances as a tool to study temperature-reliant on ductile-brittle change [16,17]. Charpy impact tests were conducted at all temperatures on the cast and rheocasting samples using a VEB machine along with a pendulum having obtainable energy of 50 J. The samples have V-notch with standard dimensions (10 mm x 10 mm x 55 mm) were used [9].

2 Metal and Methodology

The chemical compositions of the alloy used in this work are given in Table 1. The aluminum-silicon-magnesium alloy grade (Al Si1Mg Mn) is typically used for intricate and thin-walled castings of high strength demand. The functioning of the rheocasting process to produce slurries of the alloys mentioned above is described in detail in [6,10].

Table 1. The chemical composition of Aluminum EN AW 6082 alloys.

wt%	Al	Mg	Si	Cr	Fe	Mn	Cu	Ti	Zn
EN AW 6082	Bal.	0.6	0.73	0.25	0.5	0.4	0.1	0.1	0.2

This type of alloy has medium strength and excellent corrosion resistance. In plate form, EN AW 6082 alloy is generally utilized for machining [7-8]. The most common uses are scaffolding elements, rail coach pieces, offshore projects, containers, machine-building, and mobile cranes. The alloy EN AW-6082 shows good resistance to dynamic loading conditions in the aforementioned applications. The resistance is attributed to its fine-grained structure. Besides this alloy, EN AW-6082 is an expert for marine applications [18-19]. In the practical alloy EN AW 6082, aluminum alloys contents of Si and Mg range between 0.5-2.2 wt% as shown in Figure 1, generally by Si/Mg ratio of more than one. [7-17]

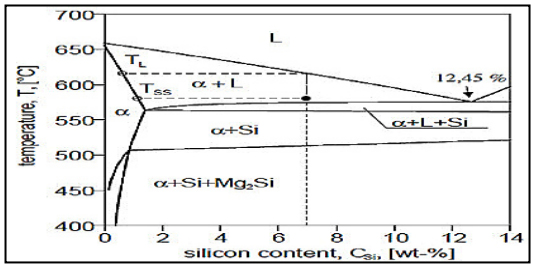

Figure 1. The phase diagram of Aluminum magnesium silicon alloys. [7]

2.1 Semi Solid Rheocasting Method

The raw material for Semi-Solid Rheocasting (SSR) is obtained directly from ingot operations, with no intermediary solidification phase. The molten metal, slightly over the liquidus temperature in Figure 2, is poured into a steel mold and then treated with the rheocasting process to generate a

globular microstructure [2].

Figure 2. Melting Aluminum magnesium silicon alloys in the mold inside the furnace and The mold for the impact the samples.

The steel mold was specifically designed for this test. In this test process, in an alloy with a Semi-Solid temperature, the molten metal is held above the liquidus temperature for a short time while the alloy rotates (low temperature). Using the steel rod in rotating motion, Semi-Solid State interacts with the liquid-solid alloy, and a temperature incline exists amid the melt and the rod. The melt on the rod's surface partially solidifies as a result of this. The nuclei are formed and subsequently thrown into the melt due to the rotating motion of the rod at alloy Semi-Solid temperature, producing a globular microstructure of tiny grains [4,11].

Figure 3.a. illustrations schematically a phase diagram and typical of an alloy composition suitable for SSM rheocasting processes. The EN AW 6082 alloy composition must prove that it results in a wide solidification interval. As well as, the process temperature (slurry temperature) must be close to the eutectic knee point temperature in liquid fraction vs. temperature curve, shown in Figure 3. b. On two sides of the knee point, a meaningful change happens in the sensitivity of solid fraction (dfs/dT) with temperature [11,14]. The reason for this is to obtain a slurry stable at the working temperature, where the solid fraction sensitivity is as minor as possible when the temperature reductions. That helps stabilize the solid fraction, as the amount of heat needed to form the eutectic phase is large [12,15].

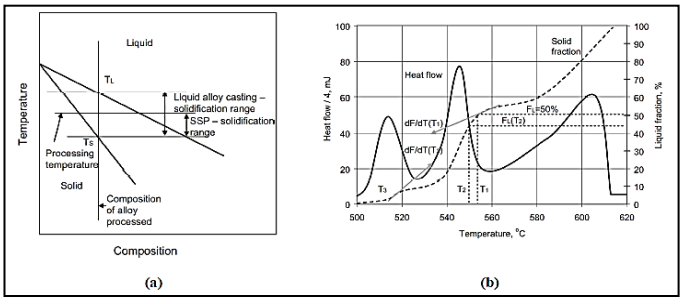

Figure 3. (a) Typical solidification range and processing temperature for SSM rheocasting, (b) Thermal analysis showing the maximum heat flow occurs at the eutectic temperature. [15]

Furthermore, the alloy composition, rotating the alloy in semi-solid temperature, and the effects of the microstructure define the final alloy properties through numerous parameters, for example, intermetallic formation, alloying elements in solid solution and their result on solidification in rheocasting processes, microstructure as well as the morphology of particles and their effect on fluidity. The consequences of adding alloying elements can be predicted by considering them as impurities or a solid solution. These have a crucial role in influencing the alloy thermal conductivity

and reducing this value intensely as the mean free path of electrons decreased significantly [14]. Since the unique metallurgical aspects of SSM casting, selecting an appropriate alloy composition must be complete so that all of these factors appropriately interact in the final product.

Both brittle and ductile fractures are archived in impact testing based on scanning electron microscopy data [20-21]. Before fracture, there was no visible plastic deformation in the brittle fracture. Furthermore, brittle fractures have less energy absorption and occur at high speeds, whereas ductile fractures have more plastic deformation before breakage [19]. Because of the absorption of a substantial amount of energy before fracture, extensive plasticity causes distorted grains around the crack to propagate slowly [21-20].

3 Result and Discussion

3.1 Charpy Impact Test

The Charpy V-test piece was used in our tests. The impact tests were performed at ambient temperature as well as at 100, 40, 25, 0, -25, -40, and -100°C. Warming to the test temperature was performed by rapid heating; the piece was put in contact with an aluminum plate preheated to the test temperature. This test uses a specimen that has dimensions of 10x10x55 mm. A notch is machined into the specimen. The V-notch design is specified in ASTM E 23 [17].

Rheocasting and casting aluminum alloys EN AW 6082 will be tested during the seven laboratory sections in which 14 specimens for each of these alloys (28 specimens in total) are studied at seven temperatures. The temperatures selected for the two types of alloys are 100, 40, 25, 0, -25, and -40 °C.

The climatic chambers for thermal shock testing are used to subject samples to simple shocks by causing them to go from a high to a low-temperature area abruptly and repeatedly. It also seeks to classify faulty components and those linked to infant mortality (mainly in the electronics sector). For a significant number of cycles, the samples are placed within a portable basket that transports them from the cold to the hot compartment and vice versa. These chambers feature two or more test compartments, and the sample is quickly passed from one to the other (usually within 10 seconds).

The temperature of the test compartments and the testing methods depend on the requirements of the standard, which defines the specific cycle to be performed.

Using temperature ACS compact test chambers, it consists of several categories with various capacities and applications, and it is also obtainable to accommodate a variety of specimen sizes. Our test chambers can simulate a wide range of temperature conditions from -40°C to 100°C (customized available, for example, constant extreme cold and hot. The specimens are moved to the Charpy testing machine easily, shattered, and assessed by the impact of energy. The fracture surfaces are inspected at the root of the notch for signs of shear or cleavage failure and lateral expansion after failure.

Figure 4 represents the variation of the energy of the value absorbed in casting and rheocasting samples at different temperatures compared to the energy absorbed in casting aluminum alloys. For energy absorbed in both aluminum alloys (casting and rheocasting) samples at 100 °C, it is showed variation from 44 to 118 Joules. At a temperature of 40°C, it is increased from 41 to 101 Joules. In the casting alloy sample, the third temperature, such as room temperature 25°C, the toughness value was 39 Joules when the toughness value increased in the rheocasting sample to 99 Joules. The energy absorbed continually increases at low temperatures starting from (0, -25, and -40) °C shows the respective casting alloy samples of 26, 22, and 18 Joules, but the toughness values in rheocasting samples are 82,80, and 75 Joules. Consequently, all Charpy Impact test rheocasting samples have high energy values due to the non-dendritic microstructure of this alloy.

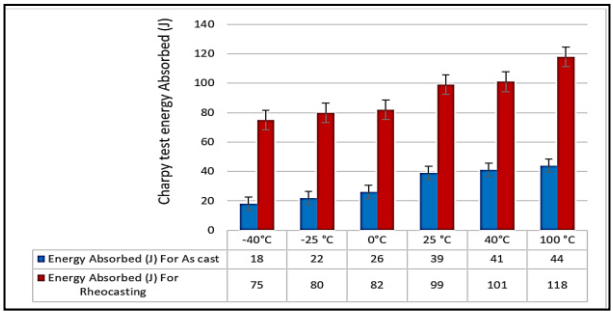

Figure 4. The energy of the value is absorbed in casting and rheocasting samples at different temperatures.

3.2 Measuring the effect of Charpy Impact Test in the samples

Figure 5 illustrates the Lateral expansion of as-cast and rheocasting Specimens at room temperatures. Measuring the cross-section of the square edge by using a digital vernier tool helps to find the effect of impact tests in the samples. The measuring cross-section of edges changes from one sample to another. These changes depend on the type of alloy and variation of temperature. Moreover, measuring the cross-section of any square edges changes following the impact test, which depends on the force acting on the specimens.

The lateral expansion is measured:

$$\Delta w = wf - wi \tag{1}$$

where *wf* is the final lateral dimension, and *wi* is the initial lateral dimension.

Figure 5. a. Lateral expansion of as-cast specimen in 25℃, b. Lateral expansion of rheocasting specimen in 25℃

3.3 Measure lateral dimensions after impact Test

The Charpy impact test sample has a square cross-section area, as illustrated in Figure 6. A specimen with dimensions of 10 x 10 x 55 mm is used in this test. A notch is cut into the specimen that measures 2 mm in total length. ASTM E 23, type A, specifies a V-notch design. Before applying loads, the edge square dimension is (10 x10) mm [3]. The edge dimension changed after finishing the test. It means that the measuring of the edge square dimension changed with the change in the type of alloy and the temperature condition. The results of the impact test show that shear characterizes a smooth surface. Cleavage and brittleness describe a fine-grained fracture surface. Failures come in many shapes and sizes (part shear and part cleavage). It's generally a brittle fracture or cleavage if there's no plastic deformation after the fracture. In an impact test, lateral expansion determines the degree of plastic deformation. The thickening of the specimen during fracture is known as lateral expansion.

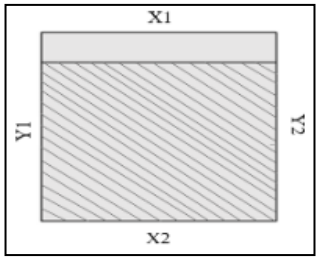

Figure 6. The standard square cross-section area of the Charpy impact test.

Figure 7 illustrates the variation of a lateral dimensions edge in the Charpy impact test in casting and rheocasting samples at a different temperature compared to the edges in casting aluminum alloys. For measuring edges in two aluminum alloys (casting and rheocasting) samples at 100 °C, the edges showed variation from (9.94, 10.14, 9.87, 10.05) mm to (9.42, 11.74, 9.44, 9.4) mm. the maximum in rheocasting sample value in the edge (X2) increased to (11.47) mm. In temperature 40°C, the edge increased from (9.9, 10.25, 10.12, 9.73) mm to (9.32, 12.01, 9.34, 9.33) mm.

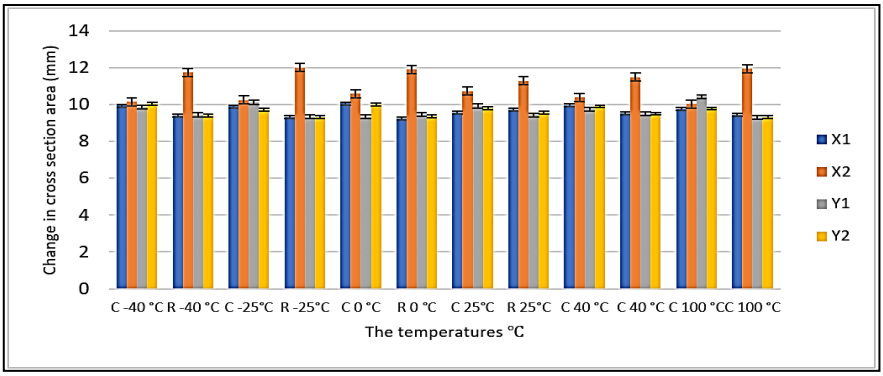

Figure 7. Bar chart measuring explosive edge in the Charpy Impact Test in casting and rheocasting samples at a different temperature.

3.4 Scanning Electron Microscope for casting and rheocasting samples at room temperature

Figures 8 and 9 show SEM images of the fracture surfaces, revealing a typical ductile and more ductile morphology for the casting and rheocasting circumstances. Both brittle and ductile fracture morphologies were seen in various portions of the impact test, and both specimens were examined at room temperature. Based on the modest Mg and Si peaks noticed in the spectrum, the energy-dispersive X-ray spectroscopy (EDS) spectrum displayed in Figure 8.b. demonstrates that these precipitates are mostly Mg_2Si precipitation. Figures 8 and 9 show comparisons of fracture surfaces acquired by SEM from impact specimens. In a ductile crystalline materials test, the fracture can happen by cleavage in the impact specimen as shown in Figure 8.a. Nevertheless, for casting impact specimen, the theory of ductile fracture is generally in grains boundaries Figure 8.b. away from the casting specimen.

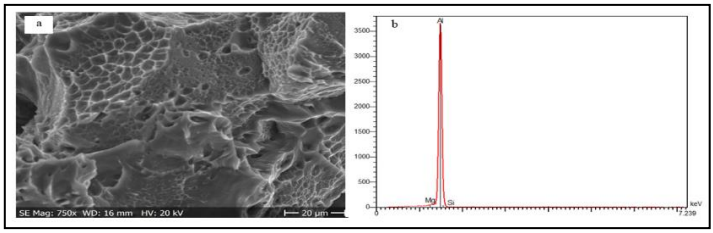

Figure 8. a. The SEM image of grain boundaries in the undeformed part of casting Specimen (39J) b. EDX spectrum revealing the precipitation of Mg2Si of casting specimen.

However, in the rheocasting impact specimen, more ductile fracture propagation among the severely deformed and elongated grains is observed to be more favorable Figure 9.a. showed the effect of more energy absorbed in the impact test compared with energy absorbed in casting specimen at room temperature. Based on the modest Mg and Si peaks identified in the spectrum, the energy-dispersive X-ray spectroscopy (EDS) spectrum displayed in Figure 9. b demonstrates that these precipitates are mostly Mg_2Si precipitation.

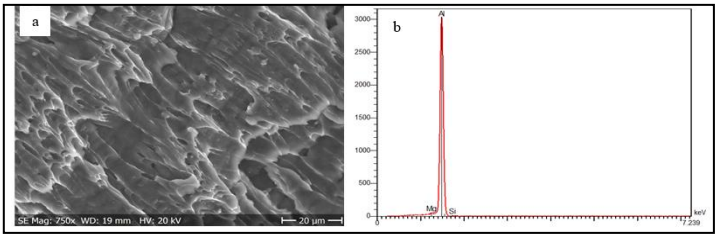

Figure 9. a. The SEM image of plastic deformation at the grain boundaries of rheocasting Specimen (99J) b. EDX spectrum revealing the precipitation of Mg2Si of rheocasting Specimen.

Because the more ductile fracture performed in the rheocasting sample impact test contains a significant degree of plastic deformation in crystallographic planes. Plastic deformation at grain boundaries is seen in Figures 10 and 11. Plastic deformation dissipates some energy from stress concentrations at grain borders, causing grain morphologies to change from spherical to longitudinal. Similar micro-cracks may also be discovered in the figure, in addition to the dimples. High Si levels were identified in the broken regions throughout the specimen, according to the EDX investigation [22].

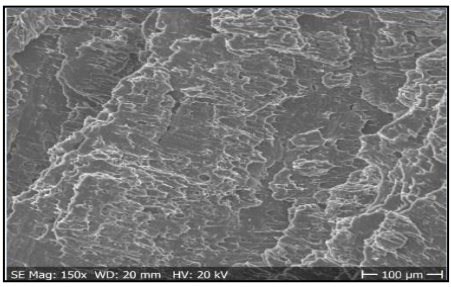

Figure 10. The ductile fracture surface of the rheocasting specimen.

Less ductile fracture typically includes little energy absorption. Figure 11 shows no more plastic deformation crystallographic planes. Mg_2Si particle precipitation does not appear to improve the alloy's impact properties; in fact, only the rheocasting sample shows an increase in the absorbed impact energy relative to the casting ones.

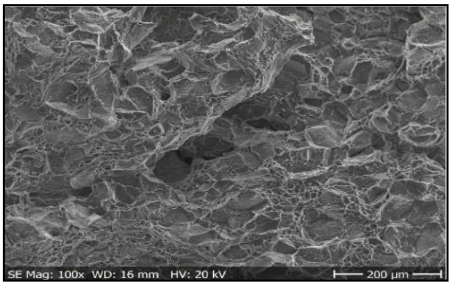

Figure 11. The less ductile cleavage fracture surface of cast Specimen from a scanning electron microscope.

3.5 Calculate Hardness Test for rheocasting and casting alloy

Figure 12 shows the hardness value of the two alloy samples. It can be noted that the sample of the rheocasting alloy has the maximum hardness followed by the casting sample. The average hardness Brinell results from rheocasting sample 125 HB and casting sample 95 HB.

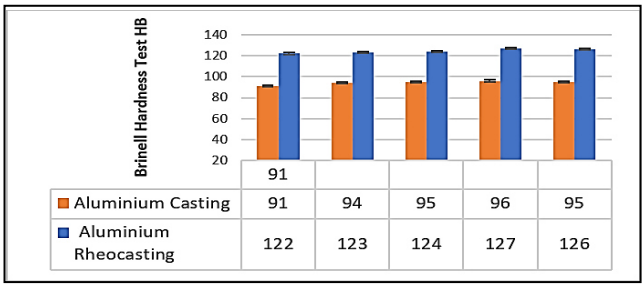

Figure 12. The average hardness Brinell of Aluminum EN AW 6082 and Rheocasting alloy.

4 Conclusions

A variety of Charpy experiments were carried out in this investigation., Impact toughness was studied for aluminum alloys EN AW 6082 containing Si and Mg in different temperature conditions. The work was conducted on two types of aluminum alloys EN AW 6082 at casting and rheocasting conduction. The investigation on aluminum alloys EN AW 6082 with casting and rheocasting specimen illustrated that the absorbed energy of the selected rheocasting aluminum alloys increases in all temperatures (100, 40, 25, 0, -25, and -40 °C) and it becomes more when it is tested in high temperatures till 100 ºC. The studies show a higher absorbed energy value in rheocasting aluminum alloy without heat treatment. The toughness value increased for the rheocasting specimens. On the contrary, the toughness decreases for the casting of aluminum alloy specimens.

- The impact of processing on the microstructure of rheocasting alloy was utilized to alter the microstructure of the two-alloy casting in response to impact findings.

- When rheocasting alloy semi-solid microstructure, the impact toughness was the highest. This process allowed significantly more non-dendrite refining, which boosted impact toughness than suction casting. Furthermore, the absorbed energy value for rheocasting specimens grew more than a repeat value in casting samples during the Charpy test in all temperature circumstances, owing to the high relative energy. All Charpy impact test rheocasting samples test has high measuring edges values compared with casting samples test shows in test Figure 4.
- The maximum value of the edges (*X2*) was in casting alloy 10.73 mm at room temperature when this value is increased to 11.29 mm in rheocasting at room temperature.
- A technique to illustrate more ductile damage is tested, which produced promising rheocasting impact results. Longitudinal grain boundaries fracture, but casting impact results showed less ductile fracture depending on the SEM analysis. Figures 8 and 9 show the SEM test for both methods.
- The average Brinell hardness test showed an increase in hardness from 95 to 125 HB for rheocasting samples.

Acknowledgments

This paper originated with the support of the Faculty of Mechanical and Safety Engineering, Hungary.

5 References

[1] J. Barson & S. Rolfe. (1970). Impact Testing of Metals, ASTM STP 466, ASTM International, West Conshohocken, PA, pp. 281–302.

[2] Hofmann, D. C., Kozachkov, H., Khalifa, H. E., Schramm, J. P., Demetriou, M. D., Vecchio, K. S. & Johnson, W. L. (2009). Semi-solid induction forging of metallic glass matrix composites. JOM 61, 11–17.

[3] Davis, J.R. (1993). ASM Speciality Handbook, Aluminum, and Aluminum Alloys, in. ASM International, Davis & Associates, Materials Park, OH. Dieter, G.E., 1986. Mechanical metallurgy, in. McGraw Hill, UK.

[4] Dowling, J.M. & Martin, J.W. (1976). The influence of Mn additions on the deformation behavior of an Al-Mg-Si alloy. Acta Metall. 24(12), 1147-1153.

[5] X. Lin, L. L. Tong, L. N. Zhao, L. L. Wang, M. Wang & W. D. Huang. (2010). Morphological evolution of non-dendritic microstructure during solidification under stirring. Transactions of Nonferrous Metals Society of China. 20, pp. 826-831.

[6] J.R. Davis, editor. ASM Specialty Handbook. (1993). Aluminum and Aluminum Alloys. ASM International, Metals Park, Ohaio, USA.

[7] Elsebaie, O., Samuel, A.M. & Samuel, F.H. (2011). Effects of Sr-modification, iron-based intermetallics, and aging treatment on the impact toughness of 356 Al-Si-Mg alloy. J Mater Sci 46, 3027-3045.

[8] Shabestari, S.G. (2004). The effect of iron and manganese on the formation of intermetallic compounds in aluminum-silicon alloys. Mater. Sci. Eng. A 383, 289–298.

[9] D. H. Kirkwood, M. Suery, P. Kapranos, H. V. Atkinson & K. P. Young. (2010) Semi-solid processing of alloys. Berlin. Springer. Vol. 124.

[10] R. Burapa, S. Janudom & T. Chucheep. (2010). Effects of primary phase morphology on mechanical properties of Al-Si-Mg-Fe alloy in semi-solid slurry casting process, Transactions of Nonferrous Metals Society of China, Vol. 20, pp. 857–861.

[11] X. Lin, L. L. Tong, L. N. Zhao, L. L. Wang, M. Wang & W. D. Huang. (2010). Morphological evolution of non-dendritic microstructure during solidification under stirring. Transactions of Nonferrous Metals Society of China. 20, pp. 826-83.

[12] Parson NC & Yiu HL. (1989). In Campbell PG, editor. Light metals. Warrendale (PA, USA) (TMS).

[13] Wang, Q.G., Davidson, C.J. 2001. Solidification and precipitation behavior of Al-Si-Mg casting alloys. J. Mat. Sci. 36, 739-750. Warmuzek, M. (2004). Aluminum-Silicon Casting Alloys - Atlas of Microfractographs, in. ASM International, Davis &Associates, Materials Park, Ohio.

[14] Hofmann, D. C., Suh, J.-Y., Wiest, A., Duan, G., Lind, M.-L., Demetriou, M. D. & Johnson, W. L. (2008) Designing metallic glass matrix composites with high toughness and tensile ductility. Nature, 451, 1085–9.

[15] ASTM Standard E23. (2007). Standard Test Methods for Notched Bar Impact Testing of Metallic Materials.

[16] Nikolaos D. Alexopoulos. (2010). Impact properties of the aircraft cast aluminium alloy Al-7Si- 0.6Mg (A357).

[17] Zhen, L., Fei, W.D., Kang, S.B. & H.W(1997). Precipitation behavior of Al-Mg-Si alloys with high silicon content. J. Mater. Sci. 32, 1895–1902.

[18] Keist, J. (2005). The development of a fluidized bed process for the heat treatment of aluminum alloys.57, 34–39.

[19] C. H. Chen, H. P. Zhang, J. Niemczura, K. Ravi-Chandar & M.(2011) Marder. Scaling of crack propagation in rubber sheets. Europhysics Letters. 96 (3): 36009.

[20] Perez, Nestor. (2016). Fracture Mechanics (2nd ed.). Springer ISBN 978-3319249971.

[21] Callister, William D. & Jr. (2018). Materials science and engineering: an introduction (8th ed.). pp. 236–237. ISBN 978-1-119-40539-9.

[22] N.D. Alexopoulos & Sp.G. Pantelakis. (2004) Metall. Mater. Trans. A, 35A, 3079.

[23] N.D. Alexopoulos & M. Tiryakio_lu. (2009) Metall. Mater. Trans. A, 40A, 716.